SURFACE AND ALOFT MEASUREMENTS OF AEROSOL CONCENTRATIONS IN A WINTERTIME BOUNDARY LAYER AT A MID-ATLANTIC SITE

Richard D. Clark[*], Daniel Brewer, Evan Lowery, Daniel Rabatin, John Yorks,
Kristin Howett, Angela Rowe, Courtney Hanna, and Maureen Maiuri
Department of Earth Sciences (Meteorology)
Millersville University of Pennsylvania, Millersville, Pennsylvania

1. INTRODUCTION

A detailed examination of the structure and evolution of the wintertime boundary layer was conducted from 3 January – 14 February 2004 near Lancaster, PA in support of the research objectives of the Mid-Atlantic/Northeast – Visibility Union (MANE-VU). Two tethered balloons were used to deploy meteorological sensors, condensation particle counters, laser-diode scatterometers, and filter samplers to altitudes of 750 m AGL, while a suite of ground-based instruments measured trace gas and particle concentrations and meteorological parameters, and where used for calibration and intercomparison with balloon-borne instruments. Sensors onboard tethered balloons used in conjunction with surface measurements can sample the boundary layer with high spatio-temporal resolution, which is essential for the characterization of the coupling between the surface and free atmosphere. Measurements were primarily limited to times when progressive anticyclones moved over the site, bringing clear skies, strong nocturnal radiational cooling, and wind speeds not exceeding the balloon capability of 12 ms^{-1}. These polar air masses influenced the meteorology and chemistry of the site/region for durations ranging from several hours to 2-3 days. This study shows that during these episodes of large-scale subsidence and relatively light winds particulates accumulate in the boundary layer and may deleteriously affect human health.

Studies of the wintertime boundary layer are rare. Much of what we know of the cold season boundary layer comes from studies in the Polar Regions (Parish and Casano 2000; Broeke et al. 2002) and the Grand Canyon (Whiteman et al. 1997). There the boundary layer forcing and chemistry are very different

than that found in the highly populated mid-Atlantic. This study is unique in that it focuses on the structure of the mid-Atlantic wintertime boundary layer and the characterization of particulates in a region influenced by two major urban areas within a 100 km radius, westerly transport from the Ohio River Valley, and local emission sources.

2. DATA COLLECTION

The Millersville University tethered atmospheric sounding system (MU-TASS), along with a suite of surface instruments, was deployed to study the wintertime boundary layer (WBL) in a Class I visibility area in the MANE-VU domain located 16.2 km SW of the Lancaster, PA airport. The site is locally representative of the rural/agricultural landscape characteristic of western Lancaster County, and regionally representative of the mid-Atlantic Piedmont.

The MU-TASS consists of a 12 m^3 blimp with a free lift capacity of 7.5 kg, which was used for vertical profiling, and a second 12 m^3, spherical balloon for long-duration time series at constant altitude. The blimp used for vertical profiling (VP) was limited to wind speeds less than 12-13 ms^{-1}, whereas the spherical balloon using for approximate constant altitude time series (CA) had a free lift capacity similar to the blimp under calm conditions, and gained lift with increasing wind speed. Over 120 vertical profiles were performed obtained using the VP blimp and 87 hours were logged on the CA balloon during six notable episodes spanning the six-week project (see Fig. 1). Each balloon platform carried a Väisälä TS111 meteorological sensor package, which recorded and transmitted temperature, pressure, relative humidity, wind speed, and wind direction to a data acquisition system at the surface where it could be displayed and archived. In addition, each ascent/descent vertical profile alternated between carrying an optical scatterometer (TSI DustTrak Model

---

[*]*Corresponding author address:* Richard D. Clark, Dept. of Earth Sciences, P.O. Box 1002, Millersville University, Millersville, PA 17551; Richard.clark@millersville.edu
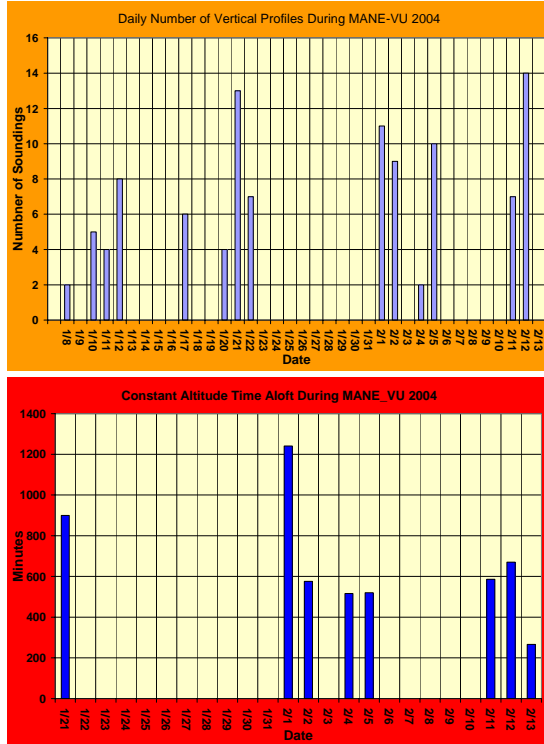
Fig. 1. The daily number of vertical profiles (top) and the daily number of total minutes (bottom) that the two Millersville tethered balloons were deployed.

8520) and a condensation particle counter (TSI Model 3007). The load was too heavy to deploy both simultaneously. The CA balloon was used to deploy an optical scatterometer as well as an SKC Personal Environmental Monitor for long-duration integrated sampling of particulates with a PM2.5 size cut. A summary of balloon-borne instrument specifications is shown in Tables 1 and 2.

Surface instruments included a portable meteorological tower for conventional atmospheric variables, a suite of three API trace gas analyzers NO/NO$_2$/NO$_X$, SO$_2$, and CO), and a TSI 3-wavelength nephelometer (Model 3563) for total and back scattering coefficient (β). Additional instrumentation included an McGee Aethalometer for BC and UV-C concentrations and a MetOne Model 9012 Ambient Aerosol particle sizer, which measured particle concentrations in six size bins ranging from 0.3 µm to greater than 0.8 µm. A summary of sensor specifications is shown in Table 3. Eta and WRF gridded data, satellite and radar imagery, surface and upper data, EPA PM2.5 data, and HYSPLIT trajectories were archived in order to later place the site measurements into a regional context.

TABLE 1: BLIMP (VP) SENSOR SPECIFICATIONS

Variable or Instrument	Method	Range	Resolution	Response Time	Repeata bility	Sampling Frequency
Temperature	Capacitive wire	-50 … + 60 C	0.1 C	0.2 s	0.10 C	1 second
Humidity	Thin film capacitor	0 …100%	0.1%	< 0.5 s @ 20 C	2%	1 second
Pressure	Silicon sensor	500 … 1080 hPa	0.1 hPa	N/A	0.4 hPa	1 second
Wind speed	3-cup anemometer	0 … 20 m/s	0.1 m/s	N/A	N/A	1 second
Wind direction	Digital compass	0 … 360 deg	1 deg	N/A	N/A	1 second
PM2.5 Conc (DustTrak Model 8520) Temp range 0 – 50 C (Calibrated for standard ISO 12103-1, A1 test dust)	90 deg Laser-diode photometry Flow Rate 1.7 L/min	0.001 … 100 mg/m^3	± .1% of reading or 0.001 mg/m^3			10 second thru 1/22/04 1 second after 1/22/04
Condensation Particle Counter (TSI Model 3007) Temp range 0 – 50 C	Cloud chamber w/ optical scatterometer Flow Rate 700 cc/min	0.01 … 1.0 µm; 0 …100,000 cm^3	1 particle cm^3			1 second

TABLE 2: BLIMP (CA) SENSOR SPECIFICATIONS

Variable or Instrument	Method	Range	Resolution	Respons e Time	Repeata bility	Sampling Frequency
PM2.5 Conc (DustTrak) Temp range 0 – 50 C (Calibrated for standard ISO 12103-1, A1 test dust)	90 deg Laser-diode photometry Flow Rate 1.7 L/min	0.001 … 100 mg/m^3	± .1% of reading or 0.001 mg/m^3	N/A	N/A	1 second thru 2/2/04 3 seconds after 2/2/04
SKC Personal Environmental Monitors for integrated filter samples	Inertial separation/im paction Gravimetric analysis Flow Rate 4 L/min	< 2.5 µm (2.5 µm size cut)	N/A	N/A	N/A	Integrated sample, 4 hours min; 10 hours max.

TABLE 3: SURFACE-BASED INSTRUMENT SPECIFICATIONS

Variable or Instrument	Method	Range	Resoluti on	Response Time	Repeat ability	Sampling Frequency
Temperature	Capacitive wire	-50 … + 60 C	0.1 C	0.2 s	0.10 C	1 minute
Humidity	Thin film capacitor	0 …100%	0.1%	< 0.5 s @ 20 C	2%	1 minute
Pressure	Silicon sensor	500 … 1080 hPa	0.1 hPa	N/A	0.4 hPa	1 minute
Wind speed	3-cup anemometer	0 … 20 m/s	0.1 m/s	N/A	N/A	1 minute
Wind direction	Digital compass	0 … 360 deg	1 deg	N/A	N/A	1 minute
PM2.5 Conc (DustTrak Model 8520) Temp range 0 – 50 C	90 deg Laser-diode photometry Flow Rate 1.7 L/min	0.001 … 100 mg/m^3	± .1% of reading or 0.001 mg/m^3	N/A	N/A	5 minute (ave)
Condensation Particle Counter (TSI Model 3007) Temp range 0 – 50 C	Cloud chamber w/ optical scatterometer Flow Rate 700 cc/min	1.01 … 1.0 µm; 0 …100,000 cm^3	1 particle cm^3	N/A	N/A	5 minute (ave)
SKC Personal Environmental Monitors for integrated filter samples	Inertial separation/impaction Gravimetric analysis Flow Rate 4 L/min	< 2.5 µm (2.5 µm size cut)	N/A	N/A	N/A	Integrated sample, 4 hours min; 10 hours max.
TSI 3-wavelength Nephelometer Model 3563 Scatter-coef of airborne particles	Optical integrating nephelometer;450 nm (blue), 550 nm (green), 700 nm (red). Flow Rate 20-200 L/min	Sensitivity Blue/green 1.0 x 10^7 m^{-1} Red/IR 3.0 x 10^7 m^{-1}	Drift Less than 2.0x10^7 m^{-1} at 30-sec ave time	< 10 sec		5 minute (ave)
CO conc API model 300A	Gas filter correlation RFNA-0193-093	0-1 ppm 0-1000 ppm	< 0.5 % of reading per EPA definition	< 10 sec per EPA definition	N/A	1 minute (ave)
SO$_2$ conc API model 100A	Fluorescence EQSA-0990-077	0-50 ppb / 0-20 ppm auto ranging	0.4 ppb RMS	< 20 sec per EPA definition	N/A	1 minute (ave)
NO$_x$ conc API model 200A	Chemiluminescence RFNA-1194-099	0-5 ppb / 0-2000 ppb user selectable	0.4 ppb RMS	< 20 sec per EPA definition	N/A	1 minute (ave)

3. OVERVIEW OF WINTER 2004

January 2004 was the 10th coldest on record in the mid-Atlantic region with a -6 F departure from normal (see Fig. 2). The month was also drier than normal with only 30% of normal precipitation (Fig. 2). In February 2004, both temperature and precipitation returned to near normal values. However, in the first half of February the temperature was still -2 F below normal and the precipitation was twice normal. For the project period from 3 January - 14 February 2004, the site experienced temperature departures of -6.6 F from normal and 9.6 mm above normal precipitation.
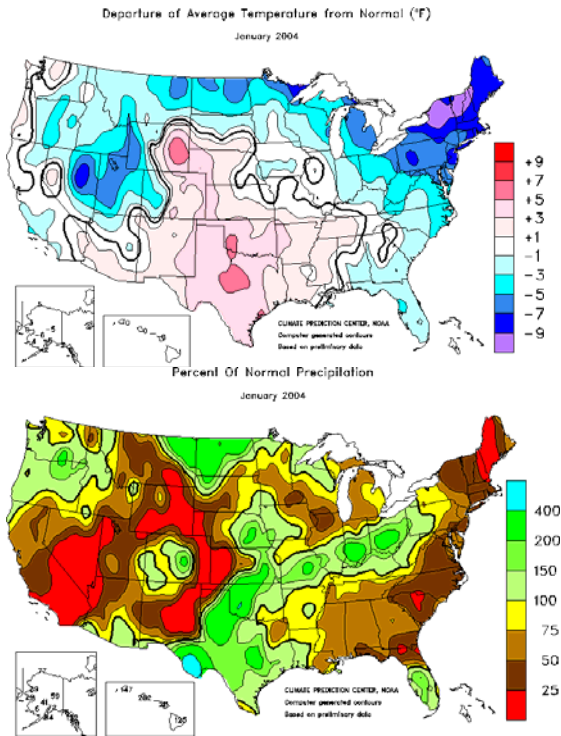
Fig. 2. Departures of temperature (top) from normal and percent of normal precipitation for January 2004.

The synoptic setting for winter 2004 was dominated by an active pattern of cyclones and anticyclones propagating over the mid-Atlantic region. From 1-27 January, the synoptic pattern has dominated by progressive Rossby waves and embedded short waves transporting frigid air from the Canadian Provinces into the mid-Atlantic, interspersed by periods of zonal flow and a return to near normal temperatures and precipitation. The climatological January thaw was absent in 2004 in this area.

A significant pattern change occurred in late January. The long-wave trough axis shifted to the Midwest and brought relatively warm, moist air into the mid-Atlantic for the remainder of the project. The contrast between the early and later periods is evident in the 300 hPa geopotential height field shown in Fig. 3. In January, continental polar and arctic air masses propagated rapidly over the area resulting in brief periods of particulate concentration enhancements typically after the passage of the ridge axis. The result was a period that was colder and drier than normal. During the latter half of the project period, the winter transport assumed a more southerly track, and one that is closer to climatology. Nonetheless, what appeared to be the

overriding factor affecting the variability of particulates and atmospheric conditions was the intrusion of the air mass and the characteristics of the circulation as it passed over the site, and not the frequency of occurrence or its source region, both of which are more important in summer. This may suggest that local and regional emissions have a greater influence on the particulate and trace gas concentrations in winter than in summer, since the rapid propagation speeds would deter long distance transport.
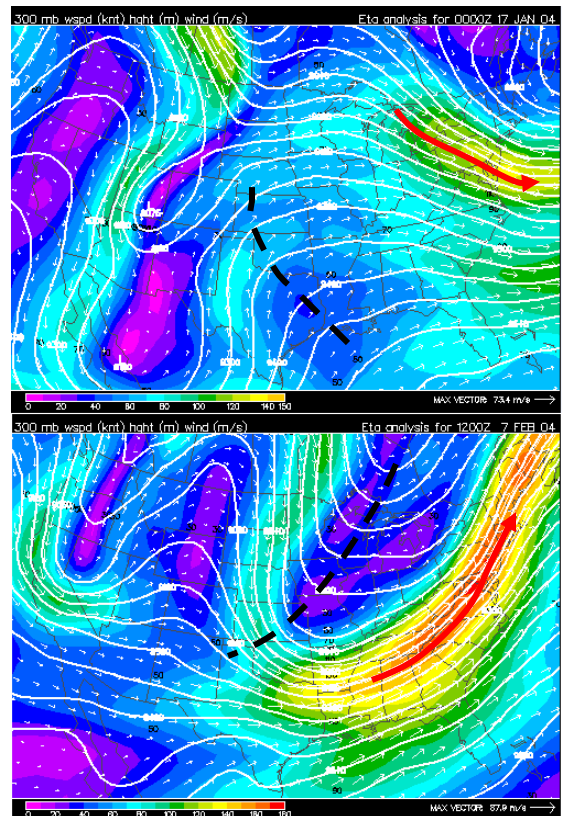

Fig. 3. The 300 hPa Eta initialization for 17 January (top) and 7 February 2004 (bottom) as an example of the differences that were observed in the synoptic pattern between the early and late periods of the study.

There are other important differences between the wintertime and summertime conditions that must be considered. The wintertime atmosphere is largely baroclinic with deep gradients, strong frontogenesis, and winds increasing with height. Shear instability is the primary turbulence production term and the source of momentum flux divergence. The forcing is often driven by upper level waves and their accompanying gradients, in contrast to summer events where the forcing is driven by differential heating in the near-surface

layers. In the daytime, momentum exchange generated by shear creates a WBL that is well-mixed and adiabatic. Winds typically increase with height throughout the mixed layer because the pressure gradient force increases with height in winter. In summer, the daytime boundary layer under conditions of high pressure is mainly driven by buoyancy production, and the horizontal winds are induced by gradients established by near-surface horizontal density (temperature) discontinuities. The height of the daytime WBL is more often determined by the tops of thermals, and boundary layer wind speed, although highly variable, is generally constant over the depth of the mixed layer.

The differences between the winter and summer nighttime boundary layer were even more pronounced. In summer, the upper levels (< 700 hPa) are barotropic, while the baroclinicity that does exist is confined to the lowest levels where gradients can form by differential heating. Conversely, with the polar jet displaced to the south and often directly over the mid-Atlantic in winter, the upper level gradients are strong and can often overwhelm boundary layer forcing, which are also diminished by the persistent wind and the effects of the lower solar insolation and reduced differential heating/cooling. A striking consequence of this difference is evident in the absence of the boundary-layer-forced low-level jet (LLJ) in winter, whereas it is a recurring feature of summertime boundary layer.

4. THE WBL DURING MANE-VU 2004

Wintertime synoptic-scale patterns have a dominating effect on the characteristics and evolution of the boundary layer through deep coupling of the upper troposphere, especially in the vicinity of fronts or during the daytime hours when the WBL is well-mixed. Atmospheric short waves like "Alberta Clippers" can bring about rapid changes in meteorological variables and particulate concentrations over periods of hours. Because of the stronger aloft gradients and attendant wind in winter, the daytime WBL more closely approximates a mechanically driven Ekman layer with a height that is largely determined by the altitude where winds reach geostrophy. On those few occasions when buoyancy plays an important role, such as during strong cold air advection in a post-

frontal environment, surprisingly deep superadiabatic layers can form between the surface and stratocumulus cloud base. The instability layer is deeper and more persistent than those generated by surface heating in summer. Particulate concentrations appear to vary inversely with wind speed, the highest concentrations are associated with light to calm winds, which adds support to the hypothesis that local and regional emissions are more important than long-range transport in winter.

Conversely, at night under strong radiative cooling, de-coupling between the WBL and free atmosphere can lead to vertical gradients in wind speed, temperature, specific humidity, and particulate concentration across sharp interfaces. At night under clear sky conditions, the cold WBL is replete with structure within and immediately above the nocturnal inversion. The inversion is often confined to a depth of only 100 meters above the surface and exhibits shallow, stably-stratified layers with pockets of high aerosol count ($\sim 10^4$ cm^{-3}) and β-scattering coefficient. Moreover, local and regional intrusions of pollutants, wind, temperature, and moisture anomalies were advected over the site and captured by the balloon measurements without the slightest trace of their existence at the surface. Thus, the wintertime boundary layer condition, not surprisingly, is one of greater diurnal contrasts, with deep coupling between the WBL during the daytime and dramatic de-coupling of the surface layers at night.

5. CASE STUDIES DURING MANE-VU 2004

Six case studies were documented between 3 January and 14 February 2004. A feature common to all episodes was the passage of a progressive high pressure system over the study area, and with it the predictable rotation of the wind from a northerly direction to a southerly direction over time. Because of the rapid propagation speed of these anticyclones, the winds were often observed to rotate as much as 270° in a matter of hours.

5a. Case Study: 2 February 2004

The 2 February 2004 case study is included as an example of the detailed WBL structure observed during MANE-VU 2004. The period is characterized by a progressive

anticyclone through the area and off the coast during the daytime hours. Fig. 4 shows the Eta initialization for 12 UTC 2 Feb (top) and 00 UTC 3 Feb 2004 (bottom). NOAA HYSPLIT back trajectories show that air parcels were advected into the region from the north (Fig. 5). The model does not capture the decidedly southwesterly flow at the surface, which backed to southeasterly between the surface and 500 m AGL. This backing is evident in the observed vertical wind profiles shown in Fig. 6, which were obtained at the site.
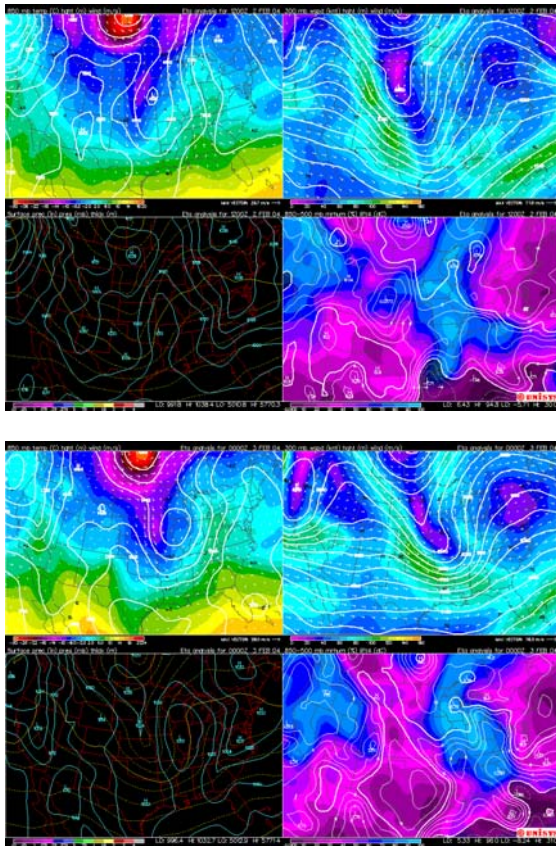
Fig. 4. Eta initializations for 12 UTC 2 Feb 2004 (top) and 00 UTC 3 Feb 2004 (bottom) illustrating the progressive movement of the mid-latitude cyclone in the Midwest toward the study area.

Fig. 7 shows air temperature measured by the vertical profiling balloon at two different times. The first profile of temperature (Fig 6 top) was obtained between 0911-0943 EST when the near-surface layers were experiencing a weak drainage flow over a snow covered surface (the site was at the bottom of a small hill rising to the southwest). The drainage resulted in mixing of a layer 50 m deep, which weakened the inversion and increased the average deviation of all

meteorological variables. This mixing marked the beginning of increases in black carbon concentration, NO_X, total scattering coefficient that persisted throughout the daytime period (Fig. 8).
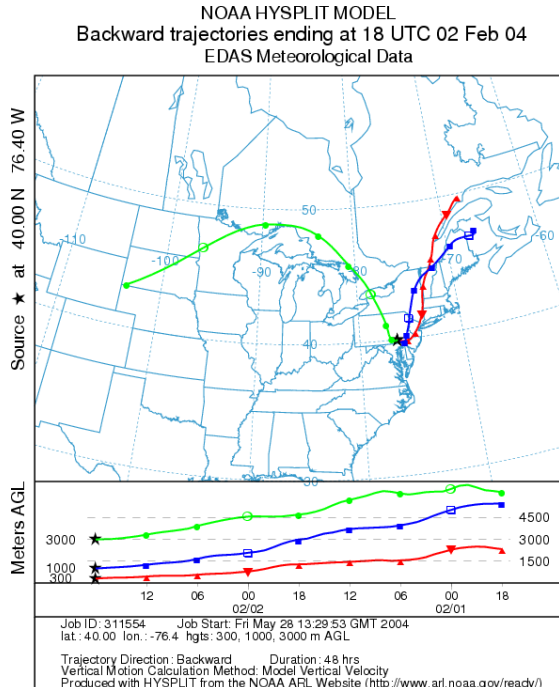

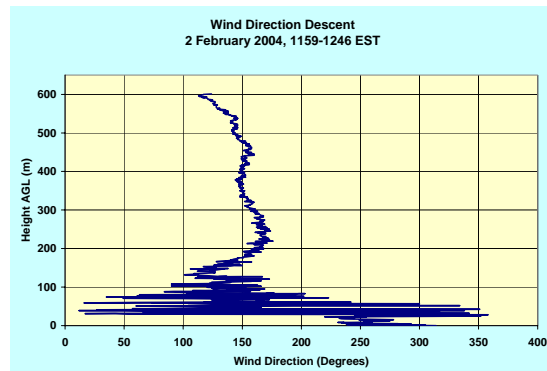Fig. 5. NOAA HYSPLIT back trajectories for 18 UTC 2 Feb 2004.
.

Fig. 6. Wind direction around noon EST 2 Feb 2004 obtained using the TASS

By 1119-1159 EST the encroachment of synoptic gradients had begun to overwhelm the local drainage. Air was transported into the region from the southeast (see Fig. 6) as continental polar air mass centered north of the Great Lakes region continued its eastward movement. The depth of the isothermal layer had increased to about 150 m with the remnant inversion remaining largely intact to 250 m AGL.

Temperature Descent
2 February 2004, 0911-0943 EST

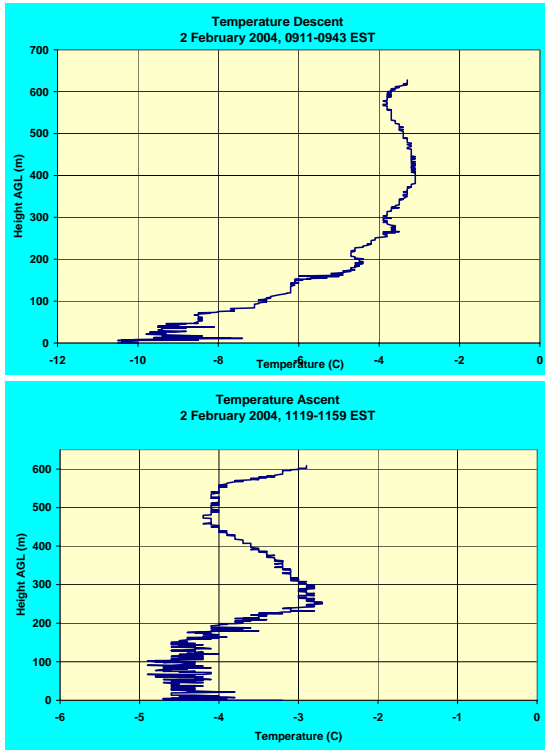**Temperature Ascent**
2 February 2004, 1119-1159 EST

Fig. 7. Temperature profile on 2 Feb 2004 at 0911-0943 EST (top); and 1119-1159 EST (bottom). Note the change in the depth of the isothermal layer.

Considerable stratification was also observed in the vertical profiles of total particle count at 0911-0943 and 1119-1159 EST (Fig. 9). The highest concentrations (16,000 cm^{-3}) were observed in the 50 m layer near the surface, and were likely due to local residential burning (i.e., coal furnaces, wood stoves) and drainage into the study area. Above the surface layer, particle counts diminish by a factor of eight in the remnant inversion before increasing again to a local maximum of 7000 cm^{-3} at 270 m AGL. This secondary peak appears to be associated with particles trapped in an aloft inversion.

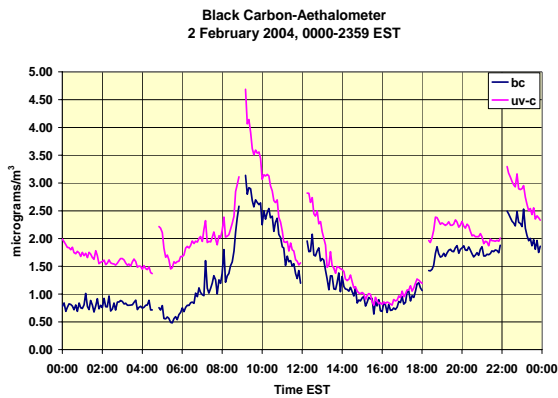**Black Carbon-Aethalometer**
2 February 2004, 0000-2359 EST

NO/NO2/NOX Concentration
2 February 2004, 0000-2359 EST

Total and Back Scattering Coefficients
2 February 2004
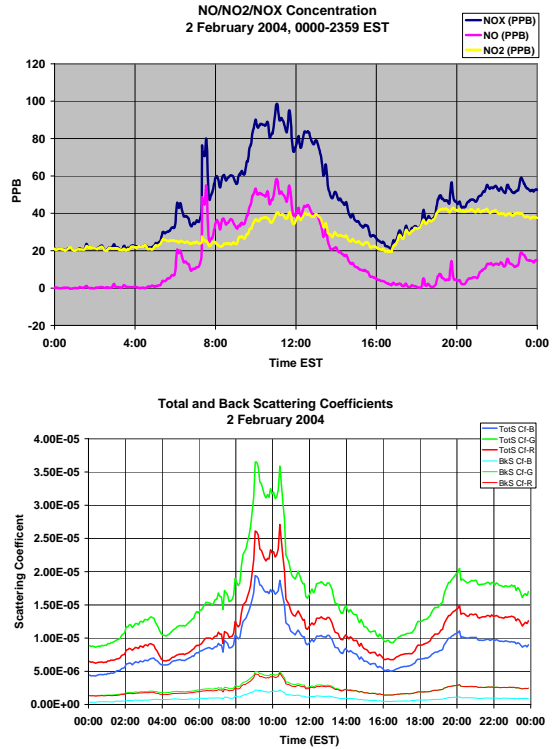
Fig. 8. Time traces of Black carbon (opposite column), NO/NO$_2$/NO$_X$, and total and back scattering coefficient for 2 Feb 2004.

Total Particle Count Descent
2 February 2004, 0911-0943 EST
TSI CPC Model 3007

Total Particle Count Ascent
2 February 2004, 1119-1159 EST
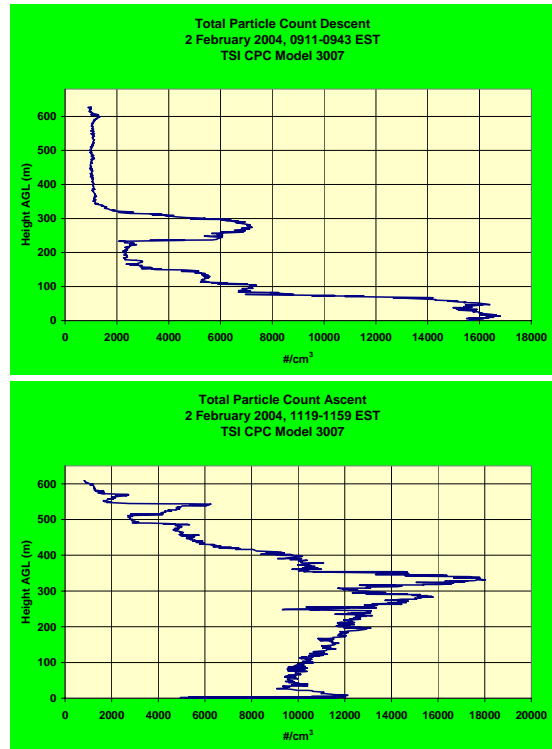**TSI CPC Model 3007**

Fig. 9. Vertical profiles of total particle count obtained using a TSI Model 3007 CPC at 0911-0943 and 1119-1159 EST.

By 1119-1159 EST, the particle count at the surface had decreased from 16,000 to 11,000 cm^{-3}, but a notable layer of high particle count was observed residing at the top of the inversion. This feature is embedded in southeasterly flow (3 ms^{-1} @ 150°) and is probably a combination of both local and regional influences, which also contributed to the elevated amounts of trace gases, scattering coefficient, and black carbon at the surface. The 2 Feb 2004 case study is characterized by an increase in aerosols and trace gases as an anticyclone moved eastward, which allowed southerly flow to become established in the lowest layers of the WBL. In a cursory way, the 2 Feb case study is reminiscent of summertime cases where the highest concentrations of particulates and traces gases are observed during the daytime period.

5b. Case Study: 5 February 2004

The case study of 5 February 2004 is an example of the influence that strong temperature inversions and local emissions sources can have on particulate matter concentrations at night, and is indicative of conditions that occur during when overcast conditions pervade during the daytime period.
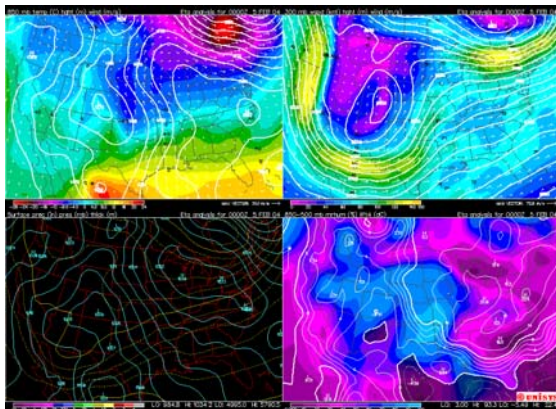

Fig. 10. Eta initialization for 00 UTC on 5 Feb 2004.

The overnight period from the 4th to the 5th of February was characterized synoptically by the passage of an extended area of high pressure over the site (Fig. 10). Clear sky conditions and strong radiational cooling helped to contribute to the 200 m AGL temperature inversion that persisted until early morning on the 5th (Fig. 11). Aloft gradients remained strong above the subsidence inversion, with wind speeds exceeding 25 ms^{-1}

at 850 hPa over the site. A 75 ms^{-1} westerly jet streak was located about 600 km north of the site, with wind speeds on the order of 40 ms^{-1} at 300 hPa over the site.
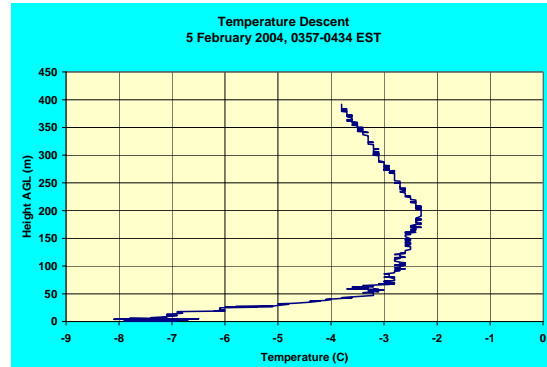

Fig. 11. Temperature profile obtained using the TASS between 0357 and 0434 on 5 Feb 2004.. Note the strong inversion from the surface to 50 m, overlain by a weaker inversion to 200 m AGL.
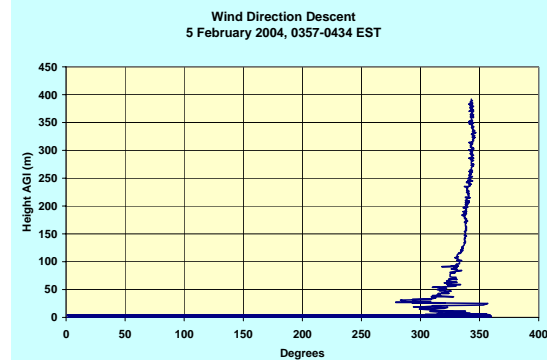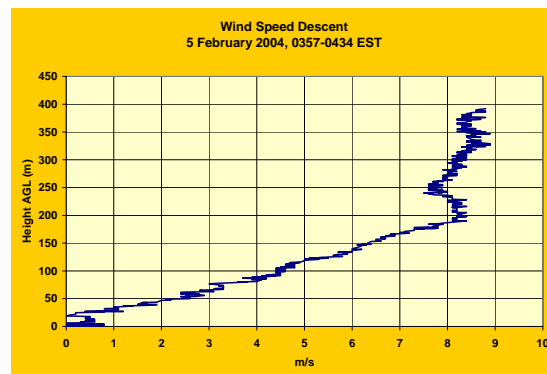

Fig. 12. Same as Fig. 11 except for wind speed (top) and wind direction (bottom).

The strength of the inversion and the shape of the temperature profile had a significant effect on stability and the consequent exchange of momentum in the lower WBL. As seen in Fig. 12 (top), winds remained calm in the lowest 25 m AGL, then increase linearly to 8.5 ms^{-1} between the surface and 200 m AGL. The

wind direction was relatively constant over the entire depth (Fig. 12 bottom). Even in the presence of relatively strong shear (3.8×10^{-2} s^{-1}), the exchange of momentum and scalars was quelled in the near surface layer. This is evidence in the vertical profile of total particle count obtained using a TSI CPC attached to the TASS, which shows that most of the aerosols were confined to the lowest 50 m AGL (Fig. 13).
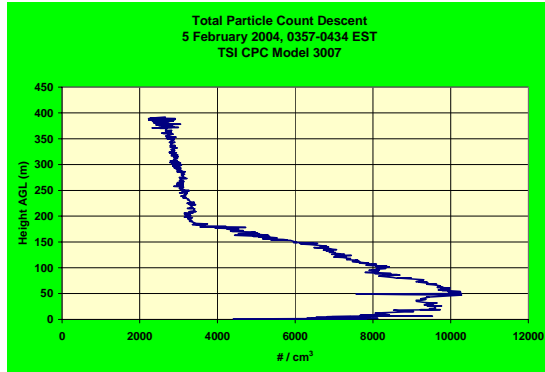

Fig. 13. Same as Fig. 11 and 12 except for total particle count obtained using a TSI Model 3007 CPC.

The stability in the lowest 50 m led to a build up of surface concentrations of black carbon, PM2.5 and total scattering coefficient at the surface, as shown in Fig. 14. Given the time of day and the wind direction, the observed concentrations are probably due to local sources. This is supported by the high UV-C concentrations observed in the Aethalometer trace, suggesting that wood smoke is an primary contributor to the non-black, UV-absorbing aromatic organic filterable material. These increases were occurring at a time of surface pressure rises and reached a maximum concentration around 0400 EST, just before a more accelerated rise in surface pressure (compare to Fig. 15).

The ridge axis moved over the site at 1200 EST, however by then, the concentrations had already begun to decrease rapidly as the surface wind increased and replaced the near surface air with cleaner, more dilated air from the north. By 1400 EST, the WBL was well mixed with uniform concentrations (e.g., PM2.5 ~ 0.025 mg m^{-3}) observed to an altitude of 500 m AGL. The vertical profiles of temperature and PM2.5 concentrations are shown in Fig. 16 for comparison. The lapse rate by mid-afternoon was approximately adiabatic over the depth of the 500 m layer.
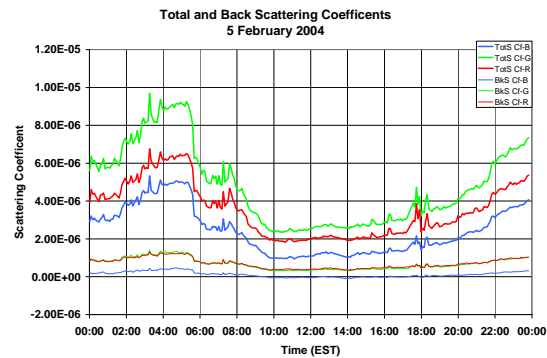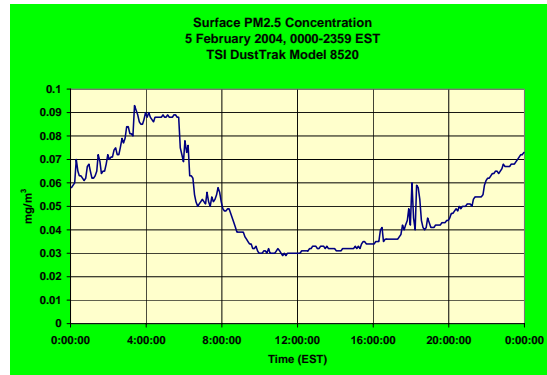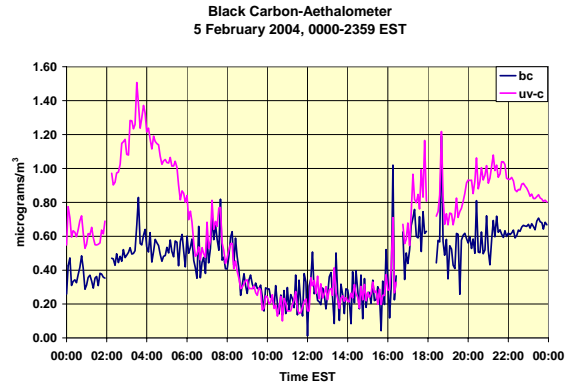

Fig. 14. Time series of black carbon (top), PM2.5 (middle), and total and back scattering coefficient (bottom) observed on 5 February 2004. The peak centered on 0400 EST appears to the result of local emissions under conditions of strong stability.
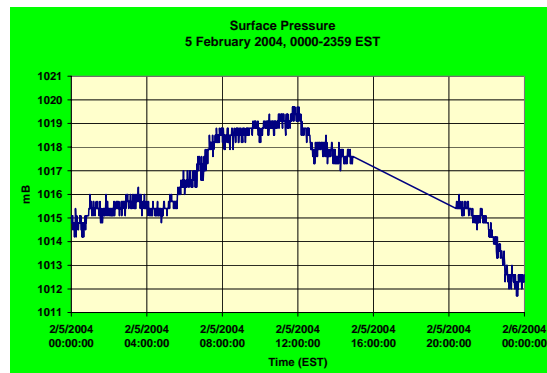

Fig. 15. Same as Fig. 14 except for surface pressure.

**Temperature Ascent
5 February 2004, 1429-1516 EST**

**PM2.5 Concentration Ascent
5 February 2004, 1429-1516 EST
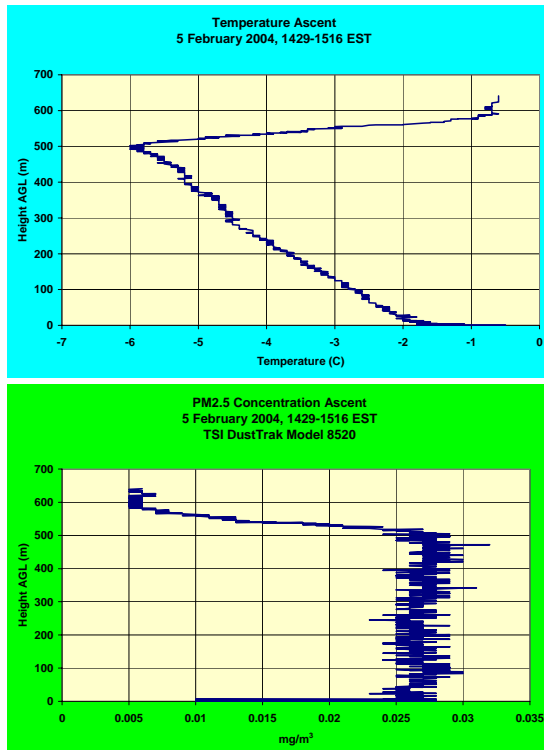TSI DustTrak Model 8520**

Fig. 16. Vertical profiles of temperature (top) and PM2.5 concentration (bottom) obtained with the TASS in mid-afternoon (1430 EST) on 5 Feb 2004.

The time series in Fig. 14 also reveal the contributions to BC/UV-C, PM2.5, and scattering coefficient from morning and afternoon traffic. The secondary peaks around 0800 and 1800 EST are the response to local traffic. The site was located adjacent to a state road that exhibited a traffic density of about two vehicles per minute during times of "high" traffic, and about one vehicle per two minutes during "low" times.

6. DISCUSSION AND SUMMARY

Four additional case studies were documented but not included in this preliminary dissemination. The two cases presented herein are by no means intended to be an exhaustive account of the complex structure and evolution of the WBL. Instead, they are intended as examples to illustrate the characteristics of the WBL, as well as to elucidate many of the problems associated with the interpretation of WBL structure and evolution. However, several noteworthy features are present in these examples that were observed throughout this winter campaign. The structure of the wintertime boundary layer is replete with detail even in

the presence of strong synoptic gradients aloft. At night under conditions of significant radiational cooling such as seen on 5 Feb, strong temperature inversions can form that quell mixing in the lowest layer, and particulate matter concentrations in the 0.01 to 1 micron range can build up in the near surface layer to values exceeding $3x10^4$ cm^{-3}, although this is still half of the summertime equivalents under conditions of strong stability. However, the strong stability present at night can be rapidly destroyed in the daytime, even though sun angles are low and solar insolation is typically less than 500 W m^{-2} in January and February. In the presence of strong baroclinicity in winter, mechanical processes in concert with weak surface heating can quickly erode the stable near surface layers and create deep adiabatic layers that drive the exchange of momentum, heat, and particulate concentrations. Whereas buoyancy dominates the forcing terms in the TKE budget in summer, mechanical production is the principal boundary layer forcing term in winter. Upper level gradients in the presence of progressive waves, strong advection, and the replacement of air masses are what characterize the winter condition. In the daytime, the wintertime boundary layer more closely resembles an adiabatic Ekman layer driven by mechanical processes (shear), with a height that is largely determine by the altitude at which the wind achieves geostrophy. In contrast, the summertime boundary layer in the daytime is largely driven by buoyancy, with the PBL height determined by the mean tops of thermals. Most of the baroclinicity in summer is induced at the surface by discontinuities that lead to differential heating and cooling. In particular, the mid-Atlantic region is subject to gradients created by the discontinuities that establish between the coastal plain and the Appalachian Mountains. Certainly, the winter landscape has its share of surface discontinuities (e.g., snow cover, land-ocean contrasts), but the reduced solar insolation combined with synoptic-scale forcing in the presence of atmospheric waves tend to diminish the establishment of persistent local and regional surface gradients.

A further example of this contrast between seasonal boundary layers is the notable lack of the boundary layer-induced low-level jet (LLJ) in winter. On only one occasion was a LLJ observed during this study, and with the

lack of upper level wind data above the site, its unequivocal existence could not be confirmed. On the other hand, the LLJ is a recurrent feature of the mid-Atlantic summertime environment formed by differential heating along the Atlantic piedmont (Clark, 2000). The LLJ forms as a complex interaction that involves the near surface gradients that give rise to a pressure gradient force that weakens with height (i.e., most of the summertime baroclinicity is generated near the surface and decreases with height), the sudden cessation of turbulent mixing around sunset, and the ensuing inertial oscillation of the wind field as it attempts to adjust to the mass field. Near surface baroclinicity as a response to differential heating is virtually absent in winter, and what there is can easily be overwhelmed by larger-scale circulations. The LLJs that do exist in winter are a misnomer. In fact, the typical wintertime "LLJ" is a transverse indirect return circulation (Dine's Compensation) induced through mass continuity in the exit region of an upper tropospheric jet located at a pressure altitude of about 850 hPa. It does not exhibit the classic inertial turning because it is entrained into the flow in a matter of hours.

That the daytime WBL is significantly influenced by larger-scale circulations and is largely mechanically driven should be an advantage for numerical modelers intent on the prediction of particulate matter variability and evolution. On the other hand, the nighttime WBL, with its highly stratified and shallow layering, complex and easily modified structure, and potential for the accumulation of high concentrations of aerosols from local source emissions, will require a deeper understanding of sub-grid scale processes. It has been the goal of this study to elucidate the characteristics of the WBL so as to glean a better understating of these processes.

The results presented herein should be considered preliminary. Considerably more work is needed and planned using the data collected during this 6-week period.

7. ACKNOWLEDGEMENTS

8. REFERENCES

Clark, R. D., C. R. Philbrick, W. F. Ryan, B. G. Doddridge, and J. W. Stehr, 2002: The effects of local and regional circulations on air pollutants during NARSTO-NE-OPS 1999-2001. *Proceedings of the Fourth Conference on Atmospheric Chemistry*, American Meteorological Society*, pp. 125-132.*

van den Broeke, M. R., N. P. M. van Lipzig and E. van Meijgaard, 2002: Momentum budget of the East Antarctica atmospheric boundary layer: results of a regional climate model. *Journ. Atmos. Sci.: Vol. 59, No. 21, pp. 3117-3129.*

Parish, T. R. and J. J. Cassano, 2001: Forcing of the wintertime Antarctic boundary layer winds from NCEP-NCAR global reanalysis. *Journ. Appl. Meteo: Vol. 40, No. 4, pp. 810-821.*

Philbrick, C. R., R. D. Clark, P. Koutrakis, J.W. Munger, B. G. Doddridge, W. C. Miller, S. T. Rao, P. Georgopoulos, and L. Newman, 2000: Investigations of ozone and particulate matter air pollution in the northeast. Preprints, *PM 2000: Particulate Matter and Health – The scientific basis for regulatory decision making.* Charleston, SC, AWMA, 4AS2; pp 1-2.

Whiteman, C. D., S. Zhong, and X. Bian, 1999: Wintertime boundary layer structure in the Grand Canyon. *Journ. Appl. Meteo: Vol. 38, No. 8, pp. 1084-1102.*